THE EVOLUTION OF LIQUID NATURAL GAS ON WATER

by

C. CARL MUSCARI
B.S.,Cornell University
1973

SUBMITTED IN PARTIAL FULFILLMENT
OF THE REQUIREMENTS FOR THE
DEGREE OF MASTER OF
SCIENCE
at the
MASSACHUSETTS INSTITUTE OF
TECHNOLOGY
August,1974

Signature of Author _____
Department of Mechanical Engineering,
August 12,1974

Certified by _____
Thesis Supervisor

Accepted by _____
Chairman,Departmental Committee on Graduate Students

THE EVOLUTION OF LIQUID NATURAL GAS ON WATER

by

C. CARL MUSCARI

Submitted to the Department of Mechanical Engineering on August 12, 1974 in partial fulfillment of the requirements for the degree of Master of Science in Mechanical Engineering.

ABSTRACT

With Euler's Equations as the starting point, appropriate physical and geometrical assumptions are made to establish the governing equations for the simultaneous spread and evaporation (burning) of a liquid natural gas (LNG) spill on water. A constant local rate of evaporation (burning) per unit area is assumed.

After non-dimensionalization, the characteristic form of these equations is derived and their numerical solution according to the method of characteristics established.

Determined from the solution are (1) the maximum radial extent of the spill, (2) duration of the entire process based on the time for complete dissipation of the spill volume, (3) graphical representations of remaining spill volume vs. time, rate of evaporation vs. time, and spill thickness vs. distance (from origin of spill) for discrete times.

Finally, an appendix outlines considerations of a similarity solution to the governing equations. The resulting proof establishes its nonexistence.

Thesis Supervisor: James A. Fay
Title: Professor of Mechanical Engineering

Acknowledgments

Requisite acknowledgment is made to my advisor, Professor James A. Fay whose incisive guidance and suggestions proved to be always fundamentally effective.

Warm and sincere thanks are extended to Ms. Sandy Williams for her kind patience and technical assistance in producing the final typed form of this work.

When, throughout the course of years that have brought me to this station in life, it seemed to me all was wavering, I sought replenishment in the inspiration and support of my family. They know I stand ever grateful before them.

Finally, ultimate gratitude must be expressed to the Sloan Foundation whose generous research traineeship has made this endeavor possible.

Table of Contents

List of Figures

List of Symbols

a, b, c, i	Subscripts denoting a point at which the dimensional or dimensionless physical quantities are to be evaluated.
F	$-(\frac{h^*U^*}{r^*} + 1)$
G	$(\frac{1}{h^*})^{\frac{1}{2}} F$
g	Gravitational constant.
$H(\eta)$	Dimensionless, local spill thickness related to a similarity variable, η.
h	Local, dimensional spill thickness.
h_{LE}	Dimensional thickness at the leading edge of the spill.
h^*	Nondimensional, local spill thickness.
h^*_{LE}	Nondimensional thickness at the leading edge of the spill.
K	A constant of integration.
$\dot{m}$	Constant mass loss rate per unit area due to <u>either</u> evaporation or evaporation and burning.
m_+	$U^*_a + (h^*_a)^{\frac{1}{2}}$
m_-	$U^*_a - (h^*_a)^{\frac{1}{2}}$
P	Local dimensional pressure of the LNG.
r	Dimensional radial co-ordinate.
R_e	Characteristic radius corresponding to t_e.
r_e	Maximum, dimensional radial extent of the spill.
r^*	Nondimensional radial co-ordinate.
t	Dimensional time.

List of Symbols (cont.)

t_e	Characteristic time of evaporation.
t_{ev}	Duration of entire spill process based on the time for complete dissipation of the initial spill volume.
t_o	Dimensional time at which the analysis of solution proceeds.
t^*	Nondimensional time.
t_o^*	The nondimensional time at which the analysis of solution proceeds.
U	Local dimensional radial velocity.
U_{LE}	Dimensional velocity at the leading edge of the spill.
U^*	Nondimensional, local radial velocity.
U_{LE}^*	Nondimensional velocity at the leading edge of the spill.
V	Initial volume of LNG spilled.
V^*	Nondimensional volume of LNG at any point in time.
v_z	Local dimensional axial velocity.
$v(\eta)$	Dimensionless, local radial velocity related to a similarity variable, η.
w	Volume loss rate per unit area.
w^*	Normalized volume loss rate per unit area = 1.
z	Dimensional axial co-ordinate.
Δ	$= (\rho_{water} - \rho)/\rho_{water}$
Δg	Effective gravity.
η	A similarity variable.

List of Symbols (cont.)

η_{max}	Value of the similarity variable at the leading edge of the spill.
λ	An experimental constant pertaining to the leading edge boundary condition (unless specified otherwise within the text).
ρ	Density of the LNG.

Introduction

In the world today, large scale transportation of natural gas over water is carried out predominantly in the liquid state (normal boiling point = -258° F) via mammoth surface vessels.

By 1980, approximately fifty LNG transport tankers are expected to be in service. Furthermore, it is anticipated that this number will continue to grow during subsequent years as the demand and resulting profitability of discovering new natural gas sources increases. The fire hazard represented by a spreading, burning pool of liquified natural gas on water due to an unscheduled release from such a tanker has been extensively examined.[1,2,3]

Upon release, the spreading liquid may either boil off violently to form a huge, volatile cloud of gas, dispersing close to the water's surface,[4] or ignition could be initiated by some random source, creating a spreading pool of fire of very high intensity but having a relatively short term.[5]

It is the intent of this thesis to develope, in as general and complete a manner deemed reasonable, a mathematical description of this spreading and simultaneous dissipation of the liquid spill, whether it be burning or evaporating. The conclusions drawn are, of course, directly applicable to any such highly evaporative fluid exhibiting the appropriate physical characteristics underlying the founding equations.

It is hoped that the significantly improved accuracy of some of its determinations (as they relate to previously published values[6]) and the new information provided by its other aspects, will be assistive to

existing and future analyses dealing with the assessment and management of the unusual fire hazards represented by LNG tanker spills.[7]

I. Formulation of the Physical Model

The mechanics of LNG spreading on water parallels to a large extent one phase in the spread of an oil spill on water. The major distinction between the two processes is the associated mass loss rate by burning or evaporation of the LNG.

The physical processes acting in the spread of an oil spill on water were first delineated by Fay[8] in his recognition of three principle regimes of flow through which the spreading film passes. They are in order:

(1) The gravity-inertia regime ("inertia spread") where the liquid spreading is caused by a hydrostatic pressure difference between the liquid and the water. This spreading force is opposed primarily, at this point, by the fluid inertia.

(2) The gravity-viscous regime ("viscous spread") wherein the friction between the spreading slick and the water below it predominates as the opposing force to the hydrostatic pressure difference.

(3) The surface tension-viscous regime ("surface tension spread") resulting from the diminishment of the hydrostatic pressure difference as the driving force and its subsequent replacement by that of the surface tension imbalance at the oil-air-water interface at the edge of the expanding slick.

Relative to the spread of LNG, only the physics of the first regime is seen to act. Before the second or third regime would be established, all of the liquid will have evaporated or burned.

There remains the question of possible freezing of the water under the spill as it evaporates. Experiments have shown that in any real spill situation, no ice is expected to form whether the pool ignites or not.[9] The assumption of a constant mass loss rate per unit area stands independent of whether ice is formed or not.

Hoult considered analytically, and in separate fashion, the description of all three regimes of flow relative to oil spreading.[10] His solution, as it pertains to inertia spread, will serve to provide the initial conditions from which the solution to the flow for all remaining time is mapped via the method of characteristics. The initial data are evaluated at a time very close to the start of the spill when the rate of evaporation (mass/time) or burning is very small (see figure 5) and as such has not significantly modified the flow from that of the non-evaporative oil spill. A complete explanation of how that solution was used in terms of the transformations between variables there and those employed here is given in appendix A.

II. Formulation of the Mathematical Model

Pertaining to the axially symmetric spread of the LNG, the general continuity equation in cylindrical co-ordinates takes the reduced form,

$$\frac{1}{r}\frac{\partial}{\partial r}(\rho r v_r) + \frac{\partial}{\partial z}(\rho v_z) = 0$$

where the approximations implied are:

(i) constant density of the liquid

(ii) The radial velocity, v_r, is considered independent of the axial direction, z.

In the development which follows, we use the notation, U, in place of v_r.

Integrating in the z-direction from 0 to h, i.e. over the thickness of the spill at any r and t:

$$\frac{1}{r}\frac{\partial}{\partial r}\int_0^h \rho r U\, dz + (\rho v_z)_h - (\rho v_z)_0 = 0$$

Noting that:

(i) $(\rho v_z)_0 = 0$

(ii) $\rho \frac{\partial h}{\partial t} = (\rho v_z)_h - \dot{m}$

where $\dot{m}$ = the constant mass loss rate per unit area due to either burning or evaporation and $\frac{\partial h}{\partial t}$ = local temporal variation of the spill thickness.

(iii) $\frac{\partial}{\partial r}\int_0^h \rho r U\, dz = \frac{\partial}{\partial r}(\rho r h U)$

and substituting accordingly, we arrive at a final form,

Continuity: $$\frac{\partial h}{\partial t} + \frac{1}{r}\frac{\partial}{\partial r}(rhU) = -\frac{\dot{m}}{\rho} \qquad (1)$$

If the right hand side of this equation were taken as zero, the result would be that derived by Hoult for the spread of an oil spill.[11]

The general momentum equation, as it pertains here, may be written,

$$\frac{\partial U}{\partial t} + U\frac{\partial U}{\partial r} = \frac{-1}{\rho}\frac{\partial p}{\partial r}$$

having used again the approximation, $\frac{\partial U}{\partial z} \simeq 0$. With the hydrostatic pressure written as $p = \rho g \Delta h$ then $\frac{\partial p}{\partial r} = \Delta\rho g \frac{\partial h}{\partial r}$, leading to the final form,

Momentum: $$\frac{\partial U}{\partial t} + U\frac{\partial U}{\partial r} = -\Delta g \frac{\partial h}{\partial r} \qquad (2)$$

This result is identical to that used by Hoult for an oil spill.

As with the case of oil, the leading edge of the LNG spill is viewed as an intrusion and as such must satisfy the boundary condition;[12]

Leading Edge: $$U_{LE} = (\lambda g \Delta h_{LE})^{\frac{1}{2}} \qquad (3)$$

where λ is a constant between 1 and 2 to be determined by experiment. Fay[13] has argued, on the basis of calculations relating to this boundary condition due to von Karman, that the value of λ should be 2. This value will be used in the calculations which follow.

It is convenient, at this point, to nondimensionalize the governing equations. From an order of magnitude analysis, the accelerating force may be taken as $F \sim (\rho g \Delta h)hR$ where R is the

spill radius. The inertia of the spill may be characterized as

$$ma \sim \rho h R^2 (R/t^2)$$

Equating the two expressions: $g\Delta h = R^2/t^2$ or $t \sim R/(g\Delta h)^{\frac{1}{2}}$.

But $h \sim V/R^2$ so that

$$t \sim R^2/(g\Delta V)^{\frac{1}{2}} \qquad (4)$$

Furthermore, $$t_e = V/(\dot{m}/\rho)R_e^2 \qquad (5)$$

is the characteristic time for the evaporation of the entire spill volume where R_e is the radius at that point in time. Elimination of R_e from equation 5 using 4 with $R=R_e$, we have,

$$t_e = [(\rho/\dot{m})(V/g\Delta)^{\frac{1}{2}}]^{\frac{1}{2}}$$

and since $R_e^2 = t_e(g\Delta V)^{\frac{1}{2}}$ we have finally

$$R_e = [(\rho/\dot{m})^{\frac{1}{2}}(g\Delta V^3)^{\frac{1}{4}}]^{\frac{1}{2}} .$$

Summarizing, the characteristic measures by which the physical quantities may be nondimensionalized are:

V = initial spill volume

$t_e = [(\rho/\dot{m})(V/g\Delta)^{\frac{1}{2}}]^{\frac{1}{2}} = [(1/w)(V/g\Delta)^{\frac{1}{2}}]^{\frac{1}{2}}$

= characteristic time of evaporation

$R_e = [(1/w)^{\frac{1}{2}}(g\Delta V^3)^{\frac{1}{4}}]^{\frac{1}{2}}$

= characteristic radius corresponding to t_e

Choosing to define:

$$r = R_e t^* \ , \ t = t_e t^* \ , \ U = \frac{R_e}{t_e} U^* \ , \ w = \frac{V}{R_e^2 t_e} w^* \ , \text{ and } \ h = \frac{V}{R_e^2} h^*$$

where the starred quantities represent nondimensional values, and substituting into equation 1:

$$(\frac{V}{R_e^2 t_e})\frac{\partial h^*}{\partial t^*} + (\frac{V}{R_e^2 t_e})\frac{h^* U^*}{r^*} + (\frac{V}{R_e^2 t_e})U^* \frac{\partial h^*}{\partial r^*} + (\frac{V}{R_e^2 t_e})h^* \frac{\partial U^*}{\partial r^*} = -(\frac{V}{R_e^2 t_e})w^*$$

and the group, $\frac{V}{R_e^2 t_e}$, is seen to divide out of the equation, leaving:

$$\frac{\partial h^*}{\partial t^*} + \frac{U^* h^*}{r^*} + U^* \frac{\partial h^*}{\partial r^*} + h^* \frac{\partial U^*}{\partial r^*} = -w^*$$

Since the group, $\frac{V}{R_e^2 t_e} = w$ (after substitution for R_e and t_e), it follows that $w^* = 1$ and thus:

$$\frac{\partial h^*}{\partial t^*} + \frac{1}{r^*} \frac{\partial}{\partial r^*}(U^* h^* r^*) = -1$$

In a similar fashion, the momentum equation may be nondimensionalized as follows:

$$(\frac{R_e}{t_e^2})\frac{\partial U^*}{\partial t^*} + (\frac{R_e}{t_e^2})U^* \frac{\partial U^*}{\partial r^*} = -\Delta g (\frac{V}{R_e^3})\frac{\partial h^*}{\partial r^*}$$

Dividing through by the group, $\frac{R_e}{t_e^2}$,

$$\frac{\partial U^*}{\partial t^*} + U^* \frac{\partial U^*}{\partial r^*} = -\Delta g (\frac{V t_e^2}{R_e^3})\frac{\partial h^*}{\partial r^*}$$

Recognizing that $\frac{gVt_e^2}{R_e^*} = 1$,

$$\frac{\partial U^*}{\partial t^*} + U^* \frac{\partial U^*}{\partial r^*} = - \frac{\partial h^*}{\partial r^*}$$

Nondimensionalizing the boundary condition, equation 3,

$$(\frac{R_e}{t_e})^2 U_{LE}^{*2} = 2g\Delta \frac{V}{R_e^2} h_{LE}^*$$

$$U_{LE}^{*2} = 2g\Delta \frac{Vt_e^2}{R_e^*} h_{LE}^* = 2h_{LE}^*$$

Summarizing, the nondimensional system of equations which is to be solved is:

Momentum: $$\frac{\partial U^*}{\partial t^*} + U^* \frac{\partial U^*}{\partial r^*} + \frac{\partial h^*}{\partial r^*} = 0 \qquad (6)$$

Continuity: $$\frac{\partial h^*}{\partial t^*} + \frac{1}{r^*} \frac{\partial}{\partial r^*}(U^* h^* r^*) = - 1 \qquad (7)$$

Leading Edge Boundary Condition: $$U_{LE}^* = (2h_{LE}^*)^{\frac{1}{2}} \qquad (8)$$

An initial attempt at solution of equations (6) through (8) involved a search for an appropriate similarity transformation which would reduce this set of equations to that of an ordinary system of differential equations. It was discovered that no such variable transformation of the form $\eta = r^{*u} t^{*v}$ for any u and v exists. The specific analysis underlying this conclusion is presented in appendix B..

Having, therefore, to operate directly on equations (6) through (8)

as a system of partial differential equations, the method of characteristics was chosen as a means of solution.

III. Solution: The Method of Characteristics[13]

Solution by the method of characteristics is very widely employed in the study of compressible fluid mechanics but is, at the same time, applicable to any two- or three- dimensional system of equations of the hyperbolic type. The defining criterion for this classification is set forth below for the case of two independent variables.

Owing to such extensive use, clear expositions on the theory underlying its application are as equally frequent and extensive.[14],[15] In light of this, the development which follows concerns itself, in most respects, only with the formalisms of the method as they apply to this particular system of equations, relying on the sources alluded to above to be assistive in the way of theory.

In addition to equations 6 through 8, we may write:

$$dU^* = \frac{\partial U^*}{\partial r^*}dr^* + \frac{\partial U^*}{\partial t^*}dt^* \qquad (9)$$

$$dh^* = \frac{\partial h^*}{\partial r^*}dr^* + \frac{\partial h^*}{\partial t^*}dt^* \qquad (10)$$

as follows from the definition of the total derivitive. Writing equations (6), (7), (9), (10) in the more expressive array,

$$h^* \frac{\partial U^*}{\partial r^*} + U^* \frac{\partial h^*}{\partial r^*} + \frac{\partial h^*}{\partial t^*} = -\left(\frac{h^* U^*}{r^*} + 1\right)$$

$$U^* \frac{\partial U^*}{\partial r^*} + \frac{\partial U^*}{\partial t^*} + \frac{\partial h^*}{\partial r^*} = 0$$

$$dr^* \frac{\partial U^*}{\partial r^*} + \frac{\partial U^*}{\partial t^*} dt^* = dU^*$$

$$dr^* \frac{\partial h^*}{\partial r^*} + dt^* \frac{\partial h^*}{\partial t^*} = dh^*$$

and letting $F = -\left(\frac{h^*U^*}{r^*} + 1\right)$, $\frac{\partial U^*}{\partial r^*}$ may be solved for using Cramer's Rule.

$$\text{Let } K = \begin{vmatrix} F & 0 & U^* & 1 \\ 0 & 1 & 1 & 0 \\ dU^* & dt^* & 0 & 0 \\ dh^* & 0 & dr^* & dt^* \end{vmatrix}$$

and

$$N = \begin{vmatrix} h^* & 0 & U^* & 1 \\ U^* & 1 & 1 & 0 \\ dr^* & dt^* & 0 & 0 \\ 0 & 0 & dr^* & dt^* \end{vmatrix}$$

then $\frac{\partial U^*}{\partial r^*} = \frac{K}{N}$.

In order to establish those directions in the r^*-t^* and U^*-h^* planes across which the respective derivitives of h^* and U^* are indeterminate, the determinants, N and K are expanded and set equal to zero.

$$N = (dr^* - U^*dt^*)dr^* - U^*dr^*dt^* + (U^{*2} - h^*)dt^{*2} = 0$$

which rearranges to form the equation,

$$\left(\frac{dr^*}{dt^*}\right)^2 - 2U^*\left(\frac{dr^*}{dt^*}\right) + (U^{*2} - h^*) = 0 \qquad (11)$$

$$K = dr^* - U^* dt^* + \left(\frac{dh^*}{dU^*} - F\,\frac{dt^*}{dU^*}\right)dt^* = 0$$

leading to the relation,

$$\frac{dh^*}{dU^*} = F\,\frac{dt^*}{dU^*} + U^* - \frac{dr^*}{dt^*} = 0 \qquad (12)$$

Equation (11) is quadratic in $\frac{dr^*}{dt^*}$ and has the solutions,

$$\frac{dr^*}{dt^*}_{\pm} = U^* \pm (h^*)^{\frac{1}{2}} \qquad (13)$$

which define the characteristic directions in the r*-t* plane. It is the fact that the radicand, $4h^*$, associated with the quadratic formula pertaining to equation (11), is greater than zero for all h^* that the system of equations is classified as hyperbolic and therefore permits solution by the method of characteristics.

If equations (13) are substituted accordingly into equation (12), the following relations result:

$$\frac{dh^*}{dU^*} = F\left(\frac{dt^*}{dU^*}\right) + (h^*)^{\frac{1}{2}} \quad \leftarrow\rightarrow \quad \frac{dr^*}{dt^*} = U^* - (h^*)^{\frac{1}{2}}$$

$$\frac{dh^*}{dU^*} = F\left(\frac{dt^*}{dU^*}\right) - (h^*)^{\frac{1}{2}} \quad \leftarrow\rightarrow \quad \frac{dr^*}{dt^*} = U^* + (h^*)^{\frac{1}{2}}$$

where "$\leftarrow\rightarrow$" indicates the substitution made. Writing these equations in the more compact notation,

$$\frac{dh^*}{dU^*} = F\left(\frac{dt^*}{dU^*}\right) \mp (h^*)^{\frac{1}{2}} \quad \leftarrow\rightarrow \quad \frac{dr^*}{dt^*} = U^* \pm (h^*)^{\frac{1}{2}}$$

Operating further on the left hand relations:

$$\left(\frac{dh^*}{dt^*}\right)\left(\frac{1}{h^*}\right)^{\frac{1}{2}} \pm \frac{dU^*}{dt^*} = F\left(\frac{1}{h^*}\right)^{\frac{1}{2}}$$

and finally we have the characteristic form of equations (6) and (7):

$$\frac{d}{dt^*}[2(h^*)^{\frac{1}{2}} + U^*] = -\left(\frac{1}{h^*}\right)^{\frac{1}{2}}\left(\frac{h^*U^*}{r^*} + 1\right) \qquad (14a)$$

$$\frac{d}{dt^*}[2(h^*)^{\frac{1}{2}} - U^*] = -\left(\frac{1}{h^*}\right)^{\frac{1}{2}}\left(\frac{h^*U^*}{r^*} + 1\right) \qquad (14b)$$

which are associated respectively with the characteristic directions,

$$\left(\frac{dr^*}{dt^*}\right)_+ = U^* + (h^*)^{\frac{1}{2}} \qquad (15a)$$

$$\left(\frac{dr^*}{dt^*}\right)_- = U^* - (h^*)^{\frac{1}{2}} \qquad (15b)$$

in the r^*-t^* plane.

If the right hand sides of equations (14) were zero then they could be directly integrated with the constants of integration evaluated at points along some line of information in the r^*-t^* plane where the values of the functions, U^* and h^* and their derivitives are known. The result would be the compatibility relations which are to be satisfied along the r^*-t^* characteristics. The network of characteristics in the h^*- U^* plane could thus be established independently from the physical characteristics of the r^*-t^* plane defined by equations (15). Furthermore, establishing the corresponding network of curves in the r^*-t^* plane would be equally facilitated by using an appropriate averaging of the physical values (U^*, h^* which would be then known) between points of inter-

section in the r^*-t^* network corresponding to the points of intersection in the completed U^*-h^* network. This,however, is not the case,with the differential form of the compatibility relations (equations (14)) being explicitly dependent on the independent variables, r^* and t^*.

For the case in question, the values of U^* and h^* at a point, $P(r^*, t^*)$, cannot be determined before the paths of the physical characteristics are known in the r^*- t^* plane. The complication is, of course, the fact that the directions of the physical characteristics, given by equations (15), are, in turn, dependent on h^* and U^*.

What this suggests is a method of successive approximations by which the r^*-t^* characteristic network and corresponding values of U^* and h^* are simultaneously mapped out forward in time from the line of initial information.

Outline of this method, as it applies here, proceeds as follows: Consider figure 1 along the horizontal line, $\overline{AB}$,corresponding to some initial time, t_o^* , where the values of U^* and h^* are known. We wish to establish the location of the point, c (along with the values of U^* and h^* there), which lies at the intersection of the plus characteristic ($\frac{dr^*}{dt^*_+}$) passing through point a and the negative characteristic ($\frac{dr^*}{dt^*_-}$) passing through point b .

Between points a and c we may write (14a) in finite difference form:

$$\frac{2[(h_c^*)^{\frac{1}{2}} - (h_a^*)^{\frac{1}{2}}] + (U_c^* - U_a^*)}{t_c^* - t_a^*} = G_{ca} \qquad (16a)$$

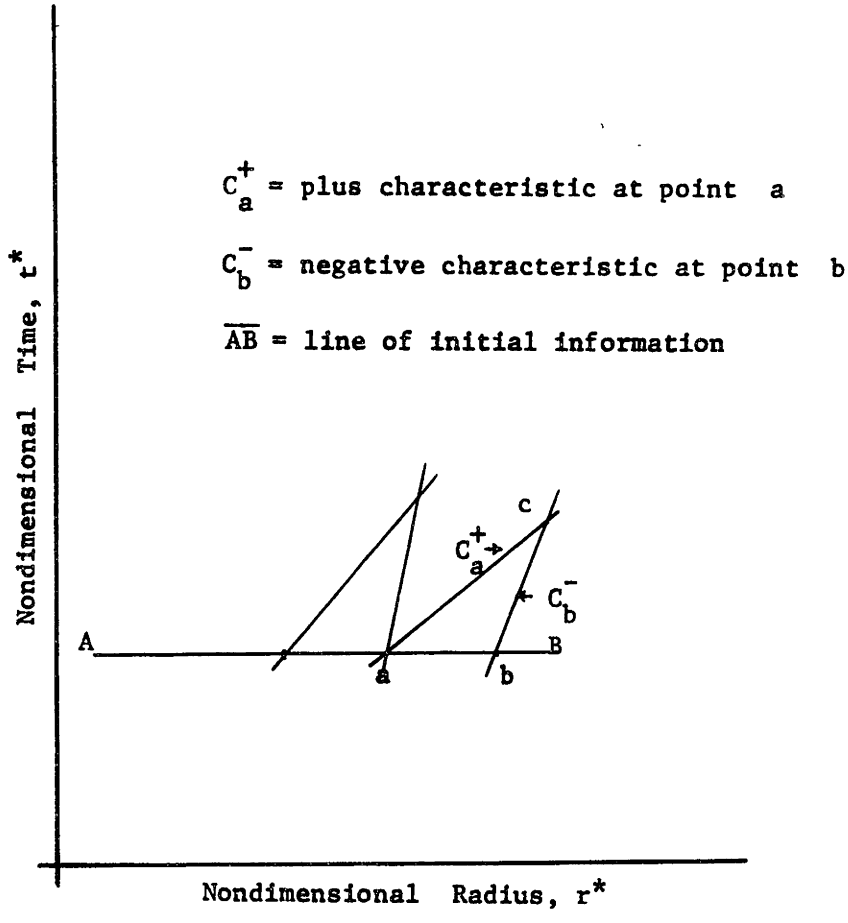

Fig. 1. Progression of the r^*- t^* Characteristic Network from the Initial Data Line.

where G_{ca} is the average value of the function, $G = (\frac{1}{h^*})^{\frac{1}{2}}F$, between points a and c . Writing (14b) in finite difference form between points b and c:

$$\frac{2[(h_c^*)^{\frac{1}{2}} - (h_b^*)^{\frac{1}{2}}] + (U_b^* - U_c^*)}{t_c^* - t_b^*} = G_{cb} \qquad (16b)$$

It is reiterated that in both of the equations, the right hand sides are evaluated at the average value of the <u>function</u>, $G = -(\frac{1}{h^*})^{\frac{1}{2}}(\frac{h^*U^*}{r^*} + 1)$, between the respective points.

Equations (16a) and (16b) may be solved simultaneously to yield expressions for h_c^* and U_c^* :

$$h_c^* = \frac{1}{16}\{-G_{ca}(t_c^* - t_a^*) - G_{cb}(t_c^* - t_b^*) - 2[(h_a^*)^{\frac{1}{2}} + (h_b^*)^{\frac{1}{2}}] + (U_b^* - U_a^*)\}^2 \qquad (17)$$

$$U_c^* = \frac{1}{2}\{G_{ca}(t_c^* - t_a^*) - G_{cb}(t_c^* - t_b^*) + 2[(h_a^*)^{\frac{1}{2}} - (h_b^*)^{\frac{1}{2}}] + (U_a^* + U_b^*)\} \qquad (18)$$

The appropriate iteration proceeds as follows:

(1) As the first approximation to the direction of the respective characteristics at a and b , the values of U^* and h^* at a and b are used in equations (15) as they apply. The resulting intersection of the characteristics provides the first estimation of r_c^* and t_c^*.

(2) With G evaluated (for the initial execution of this step only) at points a and b as they apply, and using the value of t_c^* deter-

mined in step 1, estimations of U_c^* and h_c^* are determined.

(3). The average directions of the characteristics between points a and c , and b and c are then redetermined by equations (15), using the improved values of U_c^* and h_c^* for the evaluation of the slope at point c . This leads to a more accurate location of point c . With the resulting new value of t_c^* and averaging G as it applies between the respective points, this time using the last set of values for U_c^* and h_c^* to compute G at point c ,steps two and three are repeated.

This procedure is carried out until the values of U_c^* and h_c^* are repeatable to a third decimal place. In the actual calculations made, point c would be labeled (a,b) representing the intersection of the plus and minus characteristics originating at the initial data points, a and b respectively. In this way, each intersection of the r^*-t^* network is uniquely located.

With the initial data line divided into a suitable number of discrete points, including the endpoints (labeled sequentially 1 to 33 for the calculations here), the intersections of the respective alternating plus and minus characteristics of these points are determined in the above fashion.

The right endpoint of the initial data line demands special attention

since it represents the leading edge of the spreading spill. The leading edge must move in accordance with the boundary condition, equation (8). That is, the particle path on the r^*-t^* plane corresponding to the leading edge point, must move in the direction,

$$\frac{dr^*}{dt^*} = (2h^*_{LE})^{\frac{1}{2}} \qquad (19)$$

In order that with advancing t^* the leading edge should always be located, the intersection of the plus characteristic of the point adjacent to the leading edge (the one most advanced in t^*) with the particle path is always determined. The values of r^*, t^*, h^* and U^* at the new location of the spill front are determined by somewhat different relations.

The values of U^* and h^* relating to the intersection on the r^*-t^* plane of the leading edge path and the plus characteristic of the adjacent point must satisfy equations (15a) and (19) simultaneously. Again to accurately establish this intersection an iteration procedure is required.

Considering again the three point configuration of figure 1, this time with the line $\overline{bc}$ being viewed as the endpoints of a segment of the leading edge path, the first estimate of the location of c is provided by evaluating equation (15a) with the values of h^* and U^* at a and evaluating equation (19) with the corresponding values at b. Then with $U^*_c = (2h^*_c)^{\frac{1}{2}}$ in equation (16a) and using t^*_c determined above, h^*_c and U^*_c are solved for by the relations,

$$U^*_c = [2(h^*_a)^{\frac{1}{2}} + U^*_a + G_{ac}(t^*_c - t^*_a)]/[1 + (2)^{\frac{1}{2}}] \qquad (20)$$

then

$$h_c^* = U_c^{*2}/2$$

With the new values of U_c^* and h_c^*, a better estimate of the location of point c and hence t_c^* is obtained by computing the average slope of the plus characteristic between a and c and averaging the particle direction between b and c. This scheme is also carried out until the values of U_c^* and h_c^* are repeated to the third decimal place.

After this first "advance" of intersections is determined, including the new location of the leading edge, the entire procedure is repeated successively with the newly located points (and their corresponding values of h^* and U^*) from left to right with the exception that a new boundary point is not located on the second advance. This results from the fact the the boundary point location of the first advance of intersections already lies on the plus characteristic of the point adjacent to it. It would have, therefore, its own co-ordinates as the simultaneous solution to equations (15a) and (19). Therefore, to establish the next location of the leading edge, the intersection of the plus characteristic of the right most point of intersection of the second advance with the leading edge path starting with the edge location of the first advance is required. And so it is, that a new location of the leading edge motion is provided on alternate advances of intersections. It will be noticed that under this scheme, the number of points available to establish characteristic intersections is diminished by one after alternate advances. Reference to figure 2, illustrating the actual r^*-t^* characteristic network which

resulted, will be useful in following the above discussion.

For the actual network developed, the initial data line was divided into thirty-three discrete points. The network was developed from these points. All points of intersection on this network, other than those of the indicated boundaries, are located by their characteristic co-ordinates.

The co-ordinates are determined by the characteristics which intersect there. Every characteristic starts from either the initial data line or the boundary representing the path of the leading edge. These points of origin are all numbered, with all leading edge boundary points characterized by numbers between 33 and 52 inclusively. Thus the notation, (10,35), locates the point which lies at the intersection of the plus characteristic starting at point 10 of the initial data line and the minus characteristic starting at the leading edge boundary point, 35.

A plus characteristic at any point is always distinguished from that of the minus characteristic by its more gradual slope on the r^*-t^* plane.

As each point was located, its value of U^*, h^*, r^*, and t^* were recorded and a complete table of the U^* and h^* values (as opposed to mapping a U^*-h^* network) corresponding to all points on the characteristic network is presented in appendix C. Entry to the table is made by locating the characteristic co-ordinates there, as read directly from figure 2. Any values of U^* and h^*, therefore, in the region of influence of the initial data line could be assessed via interpolation by the values of r^*, t^*, h^* and U^* relating to the nearest points of characteristic intersections.

As the spill spreads and evaporates, the thickness associated

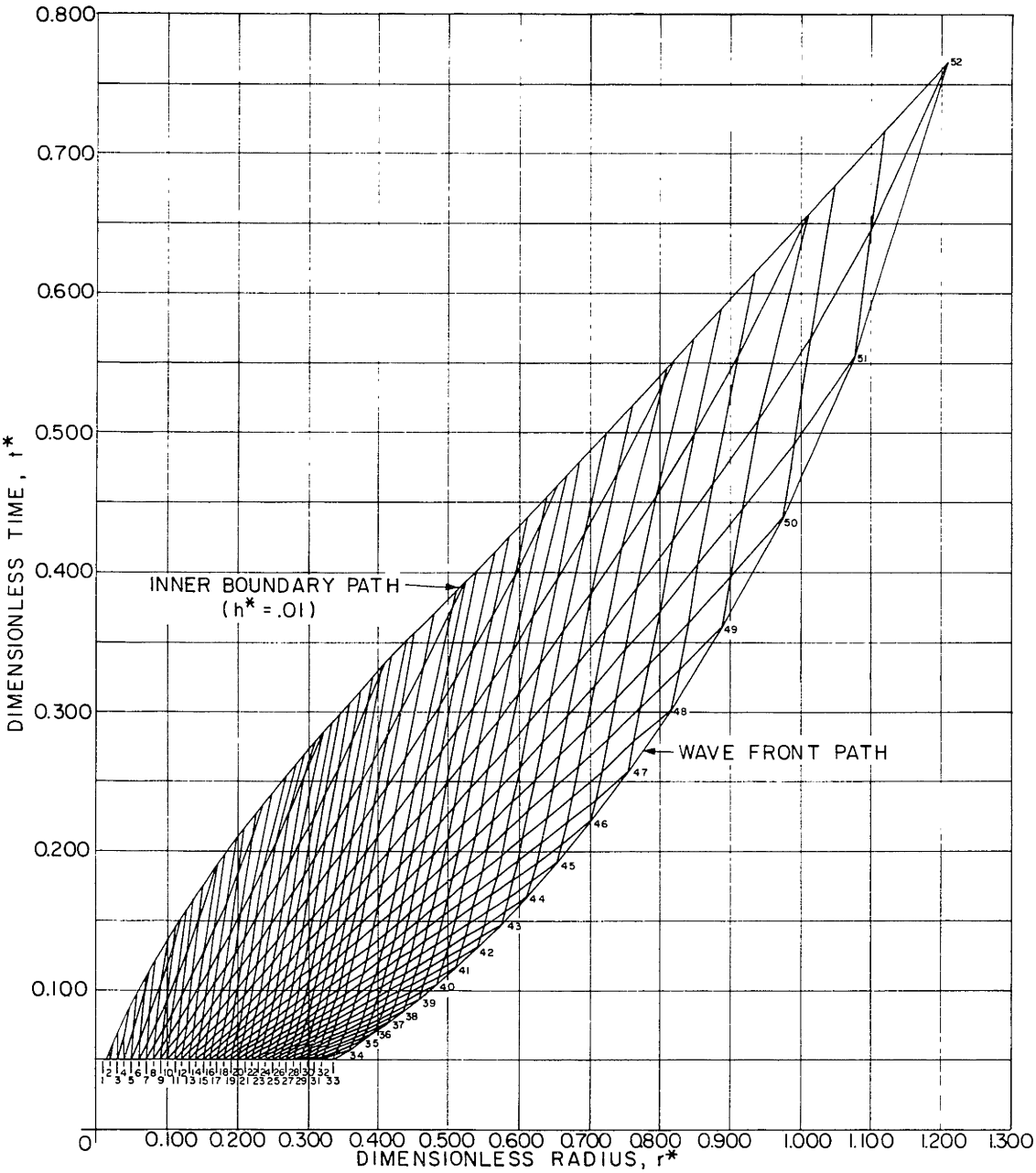

Fig. 2. The r^*-t^* Characteristic Network

with its more central regions reduces to the neighborhood of zero before the outer portions of the spill. An inner boundary to the spreading spill was established arbitrarily at those radii where h^* attained a value of less than .01 . This was necessary since, as equation (17) demonstrates, h^* may never really be computed as zero. As a result, if an arbitrary tolerance for h^* is not established the numerical solution expands to regions of physical non-relevance.

In order to insure that an adequate number of such points would be accurately located, a criterion of $h^* < .001$ was used in the calculations. That is, if a point located on the r^*-t^* plane had a value of h^* associated with it which was less then .001, it was plotted but then dropped from the calculational scheme of characteristic intersections outlined above. When all possible intersections were established, linear interpolations on radii were carried out between points having the same t^* (to two decimal places) and values of h^* surrounding and close to .01 . In many cases, values of r^* and t^* corresponding to $h^*=.01$ resulted directly from the main calculational scheme of locating characteristic intersections.

Through these points, so located, an inner boundary was drawn (see figure 2). Characteristic intersections lying outside of this boundary were then eliminated from the final illustration of the characteristic network representing the domain of influence of the initial data line.

As has been alluded to a number of times above, the procedure of solution is initiated at some finite $t^* = t_o = .05$. This starting point corresponds to the initial line of information on the r^*-t^* characteristic

plane. It is necessary that t_o^* be greater than zero since the physical model presents the entire spill process as being initiated from a point. This geometric idealization leads to unmanageable singularities in the governing equations (6) through (8) at $t^* = 0$ and $r^* = 0$. In order to circumvent difficulties of this sort, the spill process is extrapolated from $t_o^* = .05$, as opposed to $t_o^* = 0$, where it is assumed that during the interim period ($0 \leq t^* \leq .05$), the spill process is described adequately by the analytic equations of Hoult for small t^* pertaining to an oil spill on water. The validity of this assumption is dealt with in section IV. A more comprehensive discussion of this incorporation of Hoult's work, as it pertains to the initial conditions used here, is presented in appendix A.

IV. Discussion and Results

The entire calculational procedure in all its aspects, including the calculation of values pertaining to the initial data line, was computer programmed. This permitted extensive iteration leading to a highly accurate mapping of the r^*-t^* characteristic network and the determination of the corresponding values of h^* and U^*.

The completed mapping of the characteristic network appears in figure 2. In order to preserve the accuracy of the computer output, the data were plotted on graph paper permitting an accuracy of .005. As a result, the actual plot could not be included here but rather had to be first photo-reduced from an area of 13 X 16 square inches to that shown in figure 2. Owing to this, earlier (in terms of t^*) portions of the plot may appear rather nebulous.

Both the maximum radial extent (in terms of r^*) and duration of the entire spill process may be read directly from the characteristic plot as the r^*-t^* co-ordinates of the intersection of the inner (h^*= .01) and outer (leading edge path) boundaries. This particular point is labeled 52. The values corresponding to this intersection are r^*= 1.209 and t^*= .767 . These values, however, are considered to be slightly less than the true values for the process, since the connection between this point and the last located inner boundary point was a simple linear extrapolation, with the endpoint, 52, being situated at the last possible location of the leading edge.

Somewhat more accurate values are provided by the dimensionless volume (V^*) versus t^* curve (see figure 4). The extrapolated value

of t^* (a rather small extrapolation compared to that alluded to above) corresponding to zero volume is $t^* = .80$. The related value of r^* is obtained by linearly extrapolating the leading edge path on the r^*-t^* network to the point where $t^* = .80$. The corresponding value of r^* was found to be 1.23 . These values are considered more accurate because the later points on the V^*-t^* plot, pertaining to later times in the spill process, are considered to be more accurately located when compared with the points of the last portions of the inner boundary path.

The V^*-t^* plot was calculated by computing the volumes represented by the dimensionless thickness versus radial distance curves (figure 3) for discrete t^* .

In order to establish the curves of figure 3, horizontal lines were drawn on the characteristic network corresponding to the dimensionless times appearing on the figure. On these horizontal lines, an adequate number of intersections with plus and minus characteristics were located. Then for any plus characteristic intersected, the values of h^* and U^* relating to that point of intersection must satisfy equation (15a),

$$\frac{dr^*}{dt^*} = U_i^* + (h_i^*)^{\frac{1}{2}} = U_a^* + (h_a^*)^{\frac{1}{2}} = m_+ \qquad (15c)$$

and equation (16a),

$$\frac{2[(h_i^*)^{\frac{1}{2}} - (h_a^*)^{\frac{1}{2}}] + (U_i^* - U_a^*)}{t_i^* - t_a^*} = G_{ca} \qquad (16c)$$

where the subscript, i, denotes the values pertaining to the intersection of the horizontal line (i.e. the one in question) with the plus character-

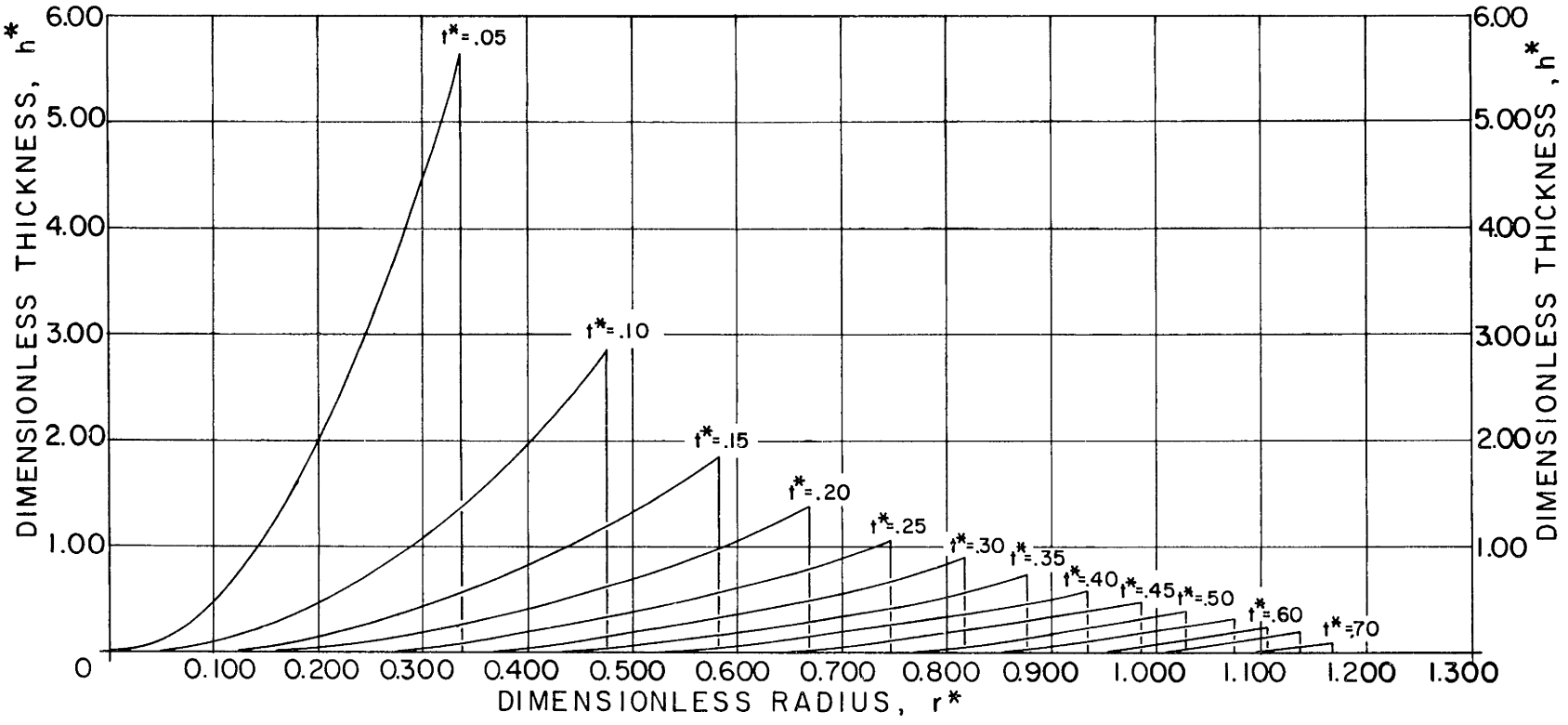

Fig. 3. Dimensionless Thickness Profiles

istic. t_i^* is, of course, known from the level on the t^* axis at which the line was drawn. The subscript, a, denotes the point representing the next characteristic intersection as one moves along the plus characteristic in question in the negative t^* direction. With respect to this point [point a], U^* and h^* have already been determined in establishing the characteristic network. The subscript, c, denotes that characteristic intersection as one moves along the plus characteristic in question in the positive t^* direction. Data pertaining to this point are also completely determined for the same reason. All these points, a,c, and i lie on the same characteristic and thus equations (15c) and (16c) result. G_{ca} is evaluated at its average value between points a and c and, therefore, the values of h_i^* and U_i^* are given by the simultaneous solution of these equations:

$$h_i^* = [G_{ca}(t_i^*-t_a^*) + 2(h_a^*)^{\frac{1}{2}} - m_+ + U_a]^2 \qquad (22)$$

then

$$U_i^* = m_+ - (h_i^*)^{\frac{1}{2}} \qquad (23)$$

In an exactly analogous fashion, the values of U^* and h^* corresponding to a point of intersection of the horizontal line with a minus characteristic must satisfy equations (15b),

$$\frac{dr^*}{dt^*} = U_i^* - (h_i^*)^{\frac{1}{2}} = U_a^* - (h_a^*)^{\frac{1}{2}} = m_- \qquad (15d)$$

and (16b),

$$\frac{2[(h_i^*)^{\frac{1}{2}} - (h_b^*)^{\frac{1}{2}}] + (U_b^* - U_i^*)}{t_i^* - t_b^*} = G_{cb}$$

where points b and c are directly analogous in direction along the minus characteristic to points a and c along the plus characteristic of the preceding discussion.

Solving equations (15d) and (16d) simultaneously:

$$h_i^* = [G_{cb}(t_i^* - t_b^*) + 2(h_b^*)^{\frac{1}{2}} + m_- - U_b^*]^2$$

$$U_i^* = m_- + (h_i^*)^{\frac{1}{2}}$$

Using these equations as they pertained, the plot of h^* vs. radial distance for t^* between .05 and .7 at intervals of .05 were established. These curves are seen to confirm the location of the inner boundary ($h^* = .01$) on the r^*-t^* characteristic plane.

The plots of V^* versus t^* and $\frac{dV^*}{dt^*}$ (rate of evaporation) versus t^* follow directly from the thickness profiles with the rate of evaporation curve being the derivitive of figure 4 . Both of these curves affirm that the approximation of utilizing the analytic solution of oil spill behavior for that of the LNG spill at small t^* is sound. This is indicated by the fact that at $t^* = .05$ (starting point of the analysis), only about .3% of the total spill volume has evaporated and the rate of evaporation has reached only about 7% of its peak value.

It might be further noted that the graph of $\frac{dV^*}{dt^*}$ versus t^* may also be viewed as the surface area of the spill versus time since a constant mass loss rate per unit area has been assumed during the development. This curve exhibits a very symmetrical behavior with a maximum, constant rate of evaporation (or surface area) attained for a

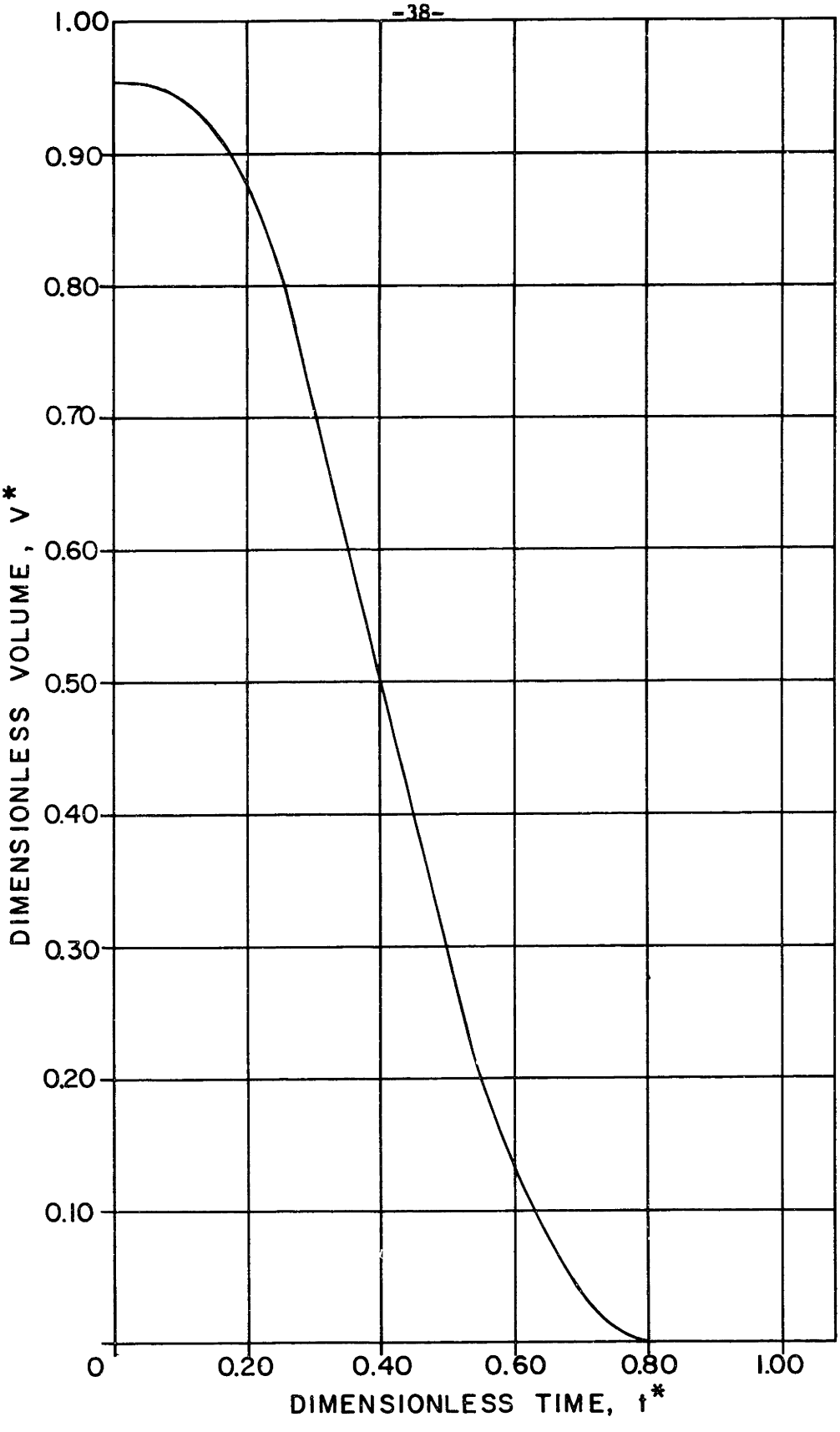

Fig. 4. Spill Volume Versus Time

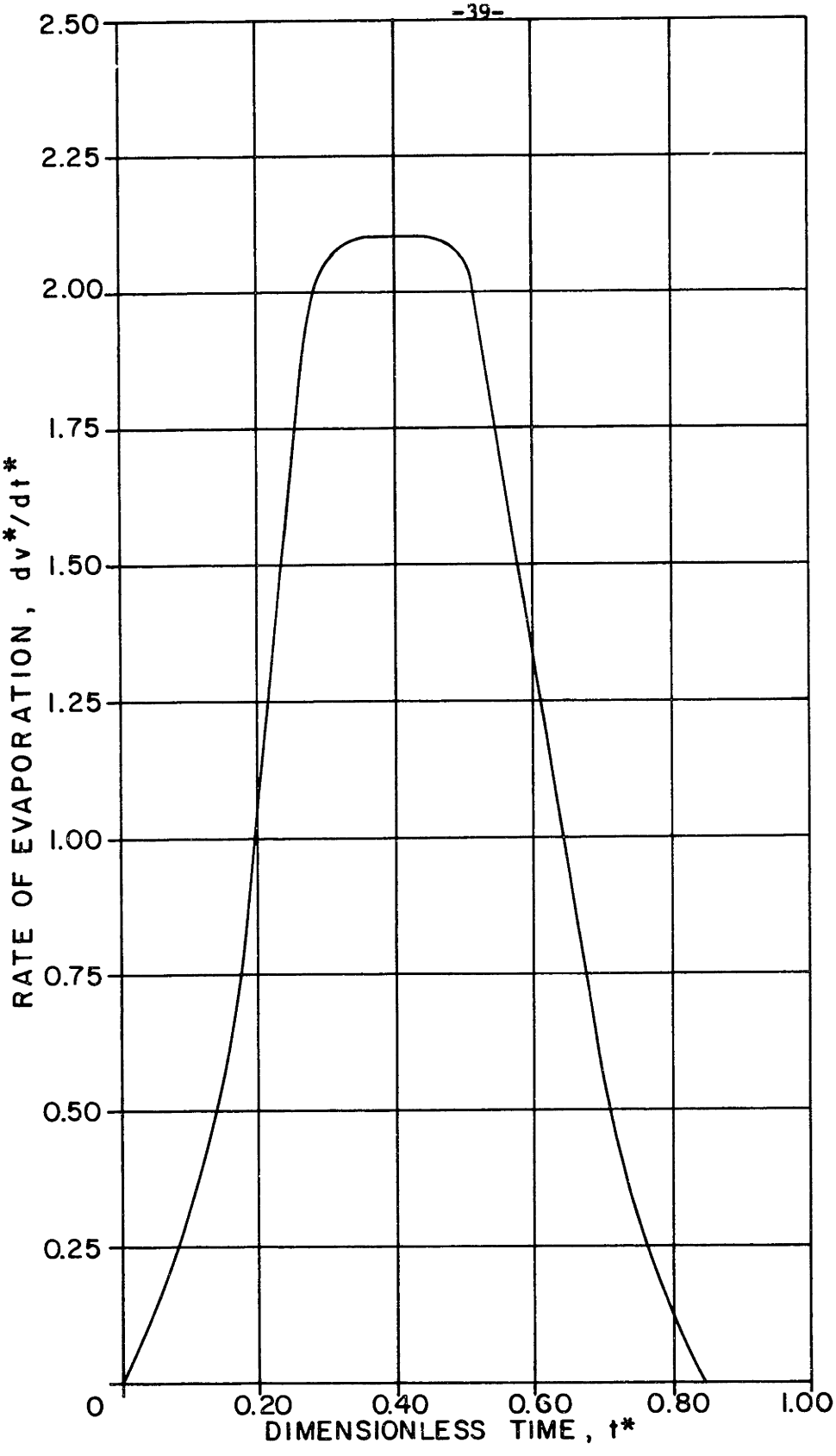

Fig. 5. Rate of Evaporation Versus Time

period of $\Delta t^* \simeq .16$.

In summary, it is concluded that the duration and maximum radial extent of the spill process are given by $t^* = .8$ and $r^* = 1.23$ respectively. Dimensionally, we have:

$$r_e = 1.23R_e = 1.23(\frac{1}{w})^{\frac{1}{4}}(g\Delta V^3)^{\frac{1}{8}}$$

$$t_{ev} = .8t_e = .8(\frac{1}{w})^{\frac{1}{2}}(\frac{V}{g\Delta})^{\frac{1}{4}}$$

Using a more finely divided initial data line at $t^* = .02$, which yields a finer characteristic network (much too fine to accurately plot), these values were found to be insignificantly altered.

These values compare to those reported by Raj and Kalelkar[16]:

$$r_e = (\frac{\lambda\rho_1}{\dot{q}})^{\frac{1}{4}}(g\Delta V^3)^{\frac{1}{8}}$$

$$t_{ev} = .67(\frac{\lambda\rho_1}{\dot{q}})^{\frac{1}{2}}(\frac{V}{g\Delta})^{\frac{1}{4}}$$

where

ρ_1 = density of the LNG

λ = heat of evaporation of the LNG

$\dot{q}$ = heat flux to the LNG

According to the authors, $\dot{q}$ is comprised of two components: heat flux due to contact with the water and heat flux due to the radiation from the fire. In this light, the group, $\frac{\lambda\rho_1}{\dot{q}}$, termed,the regression rate, is seen to be identical to the factor, $\frac{1}{w}$, as defined above and thus the non-dimensionalizations used by Raj and Kalelkar and those used

in the above development are also identical. This permits direct comparison of the values of t_{ev} and r_e.

We find, therefore, an <u>increase</u> in the predicted duration of the spill process of approximately 20% and a corresponding increase in radial extent of 23% over those values reported by Raj and Kalelkar. This, accordingly, would significantly affect the magnitudes of their assessments of safe separation distances from a burning LNG pool fire for people and combustible materials.

Literature Cited

1. Fay, J. A. Unusual Fire Hazard of LNG Tanker Spills. Combustion Science and Technology. 7:47-9. 1973.

2. Raj, P. K. P. and Kalelkar, A. S. Fire-Hazard Presented by a Spreading, Burning Pool of Liquified Natural Gas on Water. Presented at the Western States Section/The Combustion Institute 1973 Fall Meeting.

3. Hoult, D. P. The Fire Hazard of LNG Spilled on Water. Presented at the National Academy of Science Conference on LNG Importation and Terminal Safety, Boston, June 13-14, 1972.

4. Fay, Combustion Science and Technology, 47.

5. Raj and Kalelkar, 2.

6. Ibid., 8.

7. Ibid.

8. Fay, J. A. Physical Processes in the Spread of Oil on a Water Surface, in Prevention and Control of Oil Spills, American Petroleum Institute, Washington, D. C. 1971.

9. Raj and Kalelkar, 3.

10. Hoult, D. P. Oil Spreading on the Sea. Annual Review of Fluid Mechanics. 4:341-68. 1972.

11. Ibid., 345.

12. Ibid., 346-47.

13. Owczarek, J. A. Fundamentals of Gas Dynamics. International Textbook Company, Scranton, Pa. 1964, 278-303.

14. Shapiro, A. H. The Dynamics and Thermodynamics of Compressible Fluid Flow. Vol. 1. The Ronald Press Company, New York. 1953, 595-609.

15. Thompson, P. A. Compressible-Fluid Dynamics. McGraw-Hill Book Company, New York. 1972, 464-75.

16. Raj and Kalelkar, 8.

Literature Cited

17. Hoult, An. Rev. of Fluid Mech., 345-49.

Appendix A

Utilization of Hoult's Solution for Small Time

As has been pointed out (see Section III), the initial information of thickness and velocity profiles from which the entire solution was mapped out via the method of characteristics was provided by Hoult's analytic solution of the inertia spread regime of flow for the spread of an oil spill.[17] The relevant data are evaluated at a time small enough so that the flow of the LNG to this point in time may be considered to closely approximate that of the oil (see Section IV).

In his development, the following were derived as the governing equations:

Momentum: $$\frac{\partial U}{\partial t} + U\frac{\partial U}{\partial r} + g\Delta\frac{\partial h}{\partial r} = 0 \qquad (24)$$

Continuity: $$\frac{\partial h}{\partial t} + \frac{1}{r}\frac{\partial}{\partial r}(rUh) = 0 \qquad (25)$$

Leading Edge Boundary Condition: $$U_{LE} = [\lambda g \Delta h_{LE}]^{\frac{1}{2}} \qquad (26)$$

Mass Conservation: $$V = 2\pi\int_0^\infty rh\, dr = \text{constant}$$

To this system of equations, the following similarity variable was determined:

$$\eta = (g\Delta V)^{\frac{-1}{4}} r t^{\frac{-1}{2}}$$

with $$U = \frac{r}{t}v(\eta) \qquad \text{and} \qquad h = \frac{V}{r^2}H(\eta)$$

It should be noted at this point that the relations set forth in the discussion which follows will be found to be, in some respects, mildly discrepant with the analogous expressions derived by Hoult. This is attributed to an algebraic oversight on his part. The direction and motivation of the theory, however, remains identical to his.

After transformation of equations (24) through (27) and the resulting integration thereof, the following was determined:

$$v(\eta) = \frac{1}{2} \tag{27}$$

$$H(\eta) = \frac{\eta^4}{8} + K\eta^2 \tag{28}$$

where K is a constant of integration. Application of the mass constraint and the leading edge boundary condition leads to the equations,

$$K\eta_{max}^2 + \frac{\eta_{max}^4}{16} = \frac{1}{\pi} \tag{i}$$

$$\eta_{max}^4 = 4\lambda H(\eta_{max}) = \lambda\left(\frac{\eta_{max}^4}{2} + 4K\eta_{max}^2\right) \tag{ii}$$

for K and η_{max}, where η_{max} corresponds to that value of η at the leading edge where r is maximized. Hoult presented a solution to these equations for the case of $\lambda = 1$. For the problem developed here, (i) and (ii) had to be re-solved for the case of $\lambda = 2$ leading to the result:

$$\eta_{max} = 1.502 \quad \text{and} \quad K = 0$$

With respect to Hoult's development:

$$v(\eta) = \frac{t}{r} U, \quad H(\eta) = \frac{r^2}{V} h \quad \text{and} \quad \eta = (g\Delta V)^{-\frac{1}{4}} r t^{-\frac{1}{2}}$$

Pertaining to the analysis of the LNG spill:

$$U^* = (\frac{t}{R_e})U, \quad h^* = \frac{R^2}{V} h, \quad r^* = \frac{r}{R_e}, \quad t^* = \frac{t}{t_e}$$

where R_e and t_e are defined in Section II above.

Comparing the variables respectively:

$$\frac{v}{U^*} = \frac{\frac{t}{r} U}{\frac{t}{R_e} U} = (\frac{R}{t_e})(\frac{t}{r}) = \frac{t^*}{r^*} \quad \text{and thus} \quad U^* = \frac{r^*}{t^*} v$$

$$\frac{H}{h^*} = \frac{\frac{r^2}{V} h}{\frac{R^2}{V} h} = (\frac{r}{R_e})^2 = r^{*2} \quad \text{and therefore} \quad h^* = \frac{1}{r^{*2}} H$$

Now;

$$\eta^* = \frac{r^*}{(g\Delta)Vt^2} \quad \text{and} \quad R_e^* = (\frac{V}{w})(g\Delta V)^{\frac{1}{2}}, \quad t_e^2 = (\frac{1}{w})(\frac{V}{g\Delta})^{\frac{1}{2}}$$

η^* may also be written as:

$$\frac{r^4 (\frac{1}{w})(\frac{V}{g\Delta})^{\frac{1}{2}}}{(\frac{V}{w})(g\Delta V)^{\frac{1}{2}} t^2}$$

This expression, in turn, is seen to equal $\frac{r^4 t^2}{R_e^4 t^2}$ which leads, finally, to the transformation,

$$\eta = r^* (t^*)^{-\frac{1}{2}}$$

Thus we need specify t_o^* and then determine the values of h^* and U^* with the transformations between variables derived above for points

along the horizontal line on the characteristic network representing t_o^* . That is, for a given point along this line, r^* and t^* may be read directly and therefore, $\eta = r^*(t^*)^{\frac{-1}{2}}$ is determined. Then $H(\eta) = \frac{\eta^4}{8}$ (from equation (28) with $K = 0$) and $h^* = \frac{1}{r^{*2}}H(\eta)$ and $U^* = \frac{r^*}{2t^*}$ from equation (27) and the variable transformations of the preceding page. This procedure is carried out for a suitable number of points along the horizontal line, the extent of which is determined by $r^*_{max} = \eta_{max}(t_o^*)^{\frac{1}{2}}$.

Division of the line by thirty-three points for the calculations made here, was found to be "suitable" in providing a characteristic network of satisfactory detail throughout the region of influence. For purposes of calculation, the initial data line was considered to start at $r^* = .01$ in order to avoid difficulties of indeterminate division by zero relating to the compatibility relations derived in Section III .

In figure 3, the thickness profile corresponding to $t^* = .05 = t_o^*$ is the initial profile calculated from Hoult's work.

Appendix B

Considerations of a similarity Transformation

In the initial analysis of equations (6) through (8), an investigation pertaining to the possibility of a similarity variable was carried out. The existence of such a variable, meeting the leading edge boundary condition and necessary mass constraint, would have reduced the problem to a system of ordinary differential equations and, as such, would have simplified the solution. The approach used in this endeavor follows.

A similarity variable of the form,

$$\eta = r^{*u} t^{*v} \qquad (29)$$

is the initial and only assumption made. Additionally, the most general forms of h^* and U^* are postulated:

$$U^* = r^{*A} t^{*B} v(\eta) \qquad (30) \quad \text{and} \quad h^* = r^{*x} t^{*y} H(\eta) \qquad (31)$$

The unknown exponents, A, B, u, v, x and y are to be determined from the conditions of similarity which are established upon substitution of the assumed functional forms into equations (6) through (8) . This substitution results in the following expressions for Momentum:

$$Br^{*A} t^{*B-1} v(\eta) + r^{*A} t^{*B} \left(\frac{\partial \eta}{\partial t}\right) \frac{dv}{d\eta} + Ar^{*2A-1} t^{*2B} v^2(\eta) + r^{*2A} t^{*2B} \left(\frac{\partial \eta}{\partial r}\right) \frac{dv}{d\eta} v(\eta)$$

$$+ xr^{*x-1} t^{*y} H(\eta) + r^{*x} t^{*y} \left(\frac{\partial \eta}{\partial r}\right) \frac{dH}{d\eta} = 0 \qquad (32)$$

and for Continuity:

$$yr^{*x}\xi^{*y-1}H(\eta) + r^{*x}t^{*y}(\frac{\partial\eta}{\partial t})\frac{dH}{d\eta} + (A+x+1)r^{*A+x-1}t^{*B+y}H(\eta)v(\eta)$$

$$+ r^{*A+x}t^{*y+B}(\frac{\partial\eta}{\partial r})v(\eta)\frac{dH}{d\eta} + r^{*A+x}t^{*B+y}(\frac{\partial\eta}{\partial r})H(\eta)\frac{dv}{d\eta} = -1 \qquad (33)$$

and for the leading edge boundary condition:

$$r^{*2A-x}t^{*2B-y}v^2(\eta) = H(\eta) \qquad (34)$$

The conditions of similarity which determine the values of A, B, u, v, x and y are established from the requirement that each of the coefficients in equations (32) through (34) must reduce to a constant or at most a power of η . Thus, for example,

$$r^{*A}t^{*B}(\frac{\partial\eta}{\partial t}) = \eta^c = r^{*uc}t^{*vc} \qquad (35)$$

(noting that $\frac{\partial\eta}{\partial t} = vr^{*u}t^{*v-1}$ from equation (29)) for the coefficient of the second term in equation (32) . It is important to note that c itself becomes an unknown exponent. In this manner, a system of sixteen non-linear , algebraic equations may be formed by equating exponents of like variables in each such statement of constancy or power of η (equation (35)). This seemingly overwhelming set of equations reduce easily, however (by appropriate operation), to three linear equations which are independent and establish the necessary relationships between A and B, x and y, and u and v which must be met for similarity to exist. They are:

$$3x + 2y = 2 \qquad (36)$$

$$3A + 2B = 1 \qquad (37)$$

$$\frac{u}{v} = \frac{-2}{3} \qquad (38)$$

The additional unknown exponents introduced by equation of the coefficients in equations (32) through (34) with powers of η are defined once the conditions of (36) through (38) are met.

There remains, however, an additional constraint in the formulation of this approach to the problem which is that of global mass conservation:

$$V = 2\pi \int_0^{R^*(t^*)} r^* h^* \, dr^* + \pi \int_0^{t^*} R^{*2}(t^*) \, dt^* = \text{constant} \qquad (39)$$

where $R^*(t^*)$ is the leading edge, nondimensional radius. With $\eta = r^{*u} t^{*v}$; $d\eta = u r^{*u-1} t^{*v} dr^*$ and

$$dr^* = \left(\frac{1}{u}\right) r^{*1-u} t^{*-v} d\eta \qquad (i)$$

When $\eta = \eta_{max}$ then $r^* = R^*(t^*)$, that is, $R^*(t^*) = (t^{*-v} \eta_{max})^{\frac{1}{u}}$ which leads to

$$R^*(t^*) = t^{*\left(\frac{2v}{u}\right)} \eta_{max}^{\left(\frac{2}{u}\right)} \qquad (ii)$$

Remembering that $h^* = r^{*x} t^{*y} H(\eta)$ and substituting (i) and (ii) into equation (39):

$$V = \frac{2\pi}{u} \int_0^{\eta_{max}} (r^{*x+2} t^{*y}) H(\eta) \frac{d\eta}{\eta} + \pi \int_0^{t^*} t^{*\left(\frac{2v}{u}\right)} \eta_{max}^{\left(\frac{2}{u}\right)} dt^*$$

$$V = \frac{2\pi}{u} \int_0^{\eta_{max}} (r^{*x+2} t^{*y}) H(\eta) \frac{d\eta}{\eta} + \frac{(\pi u \eta_{max})^{\left(\frac{2}{u}\right)} t^{*\left(\frac{u-2v}{u}\right)}}{(u - 2v)} \qquad (40)$$

It is easily shown that the factor, $r^{*x+2} t^{*y}$, of equation 40, to be constant or a power of η, implies a relationship between x and y

which is directly inconsistent with that of equation (36) .

More obvious, however, is the fact that the explicit t^* dependence of the second term of equation (40) cannot be eliminated in a fashion consistent with the established requirement of equation (38) . That is, neither u or $(u-2v)$ may be set to zero.

It is therefore concluded that an appropriate similarity transformation of the form, $\eta = r^{*u}t^{*v}$, for the system of governing equations (6), (7), (8) and (39) does not exist.

Appendix C

Tabular Solution Pertaining to the r^*-t^* Characteristic Network

		NEGATIVE CHARACTERISTIC					
PLUS CHARACTERISTIC		2	3	4	5	6	7
2	$h^*=$	0.020	0.000				
	$U^*=$	0.200	0.164				
3	$h^*=$		0.045	0.033	0.043	0.000	
	$U^*=$		0.300	0.278	0.228	0.452	
4	$h^*=$			0.080	0.054	0.022	0.049
	$U^*=$			0.400	0.379	0.356	0.349
5	$h^*=$				0.125	0.101	0.078
	$U^*=$				0.500	0.480	0.461
6	$h^*=$					0.180	0.157
	$U^*=$					0.600	0.580
7	$h^*=$						0.245
	$U^*=$						0.700

Tabular Solution Pertaining to the r^*-t^* Characteristic Network

PLUS CHARACTERISTIC		NEGATIVE CHARACTERISTIC					
		8	9	10	11	12	13
4	h^*=	0.131	0.000				
	U^*=	0.665	1.107				
5	h^*=	0.054	0.024	0.001			
	U^*=	0.440	0.420	0.399			
6	h^*=	0.135	0.115	0.094	0.073	0.050	0.006
	U^*=	0.562	0.544	0.527	0.510	0.491	0.491
7	h^*=	0.221	0.200	0.180	0.161	0.143	0.124
	U^*=	0.680	0.662	0.646	0.630	0.614	0.599
8	h^*=	0.320	0.296	0.274	0.254	0.234	0.216
	U^*=	0.800	0.780	0.762	0.764	0.730	0.716
9	h^*=		0.405	0.380	0.357	0.336	0.316
	U^*=		0.900	0.880	0.862	0.846	0.830
10	h^*=			0.500	0.473	0.449	0.427
	U^*=			1.000	0.980	0.962	0.946
11	h^*=				0.605	0.577	0.552
	U^*=				1.100	1.080	1.062
12	h^*=					0.720	0.690
	U^*=					1.200	1.180
13	h^*=						0.845
	U^*=						1.300

Tabular Solution Pertaining to the r^*-t^* Characteristic Network

PLUS CHARACTERISTIC		NEGATIVE CHARACTERISTIC				
		14	15	16	17	18
6	h^*=	0.000				
	U^*=	0.366				
7	h^*=	0.105	0.085	0.064	0.036	0.211
	U^*=	0.584	0.569	0.553	0.538	0.748
8	h^*=	0.199	0.181	0.164	0.147	0.130
	U^*=	0.702	0.688	0.675	0.662	0.648
9	h^*=	0.297	0.280	0.263	0.246	0.230
	U^*=	0.816	0.802	0.789	0.776	0.764
10	h^*=	0.406	0.387	0.369	0.351	0.334
	U^*=	0.930	0.915	0.902	0.889	0.876
11	h^*=	0.528	0.506	0.486	0.466	0.448
	U^*=	1.045	1.030	1.015	1.001	0.988
12	h^*=	0.664	0.639	0.615	0.594	0.573
	U^*=	1.162	1.145	1.129	1.114	1.100
13	h^*=	0.814	0.785	0.759	0.734	0.711
	U^*=	1.280	1.262	1.245	1.228	1.213
14	h^*=	0.980	0.947	0.917	0.889	0.863
	U^*=	1.400	1.380	1.362	1.344	1.328
15	h^*=		1.125	1.090	1.058	1.029
	U^*=		1.500	1.480	1.461	1.444
16	h^*=			1.280	1.244	1.210
	U^*=			1.600	1.580	1.561
17	h^*=				1.445	1.407
	U^*=				1.700	1.680
18	h^*=					1.620
	U^*=					1.800

Tabular Solution Pertaining to the r^*-t^* Characteristic Network

NEGATIVE CHARACTERISTIC

PLUS CHARACTERISTIC			19	20	21	22	23
7		h^*=	0.086	0.073	0.056	0.027	0.000
		U^*=	0.986	0.976	0.973	0.999	1.028
8		h^*=	0.112	0.093	0.072	0.047	0.028
		U^*=	0.635	0.621	0.608	0.594	0.558
9		h^*=	0.214	0.198	0.182	0.166	0.149
		U^*=	0.752	0.740	0.729	0.717	0.706
10		h^*=	0.318	0.302	0.286	0.271	0.256
		U^*=	0.864	0.852	0.841	0.830	0.820
11		h^*=	0.430	0.414	0.397	0.382	0.366
		U^*=	0.975	0.963	0.952	0.941	0.930
12		h^*=	0.554	0.535	0.518	0.501	0.484
		U^*=	1.087	1.074	1.062	1.050	1.039
13		h^*=	0.690	0.669	0.649	0.631	0.613
		U^*=	1.200	1.186	1.173	1.160	1.149
14		h^*=	0.838	0.815	0.793	0.772	1.259
		U^*=	1.313	1.298	1.284	1.271	1.259
15		h^*=	1.001	0.975	0.950	0.927	0.905
		U^*=	1.423	1.412	1.397	1.383	1.370
16		h^*=	1.179	1.149	1.122	1.095	1.070
		U^*=	1.544	1.527	1.511	1.496	1.482
17		h^*=	1.371	1.338	1.307	1.278	1.250
		U^*=	1.661	1.643	1.627	1.611	1.596
18		h^*=	1.580	1.543	1.508	1.475	1.444
		U^*=	1.780	1.761	1.743	1.726	1.710
19		h^*=	1.805	1.763	1.724	1.687	1.653
		U^*=	1.900	1.880	1.861	1.843	1.826
20		h^*=		2.000	1.956	1.915	1.877
		U^*=		2.000	1.980	1.961	1.943

Tabular Solution Pertaining to the r^*-t^* Characteristic Network

PLUS CHARACTERISTIC		NEGATIVE CHARACTERISTIC				
		24	25	26	27	28
8	h^*=	0.001				
	U^*=	0.592				
9	h^*=	0.132	0.114	0.096	0.075	0.050
	U^*=	0.694	0.682	0.670	0.657	0.646
10	h^*=	0.241	0.226	0.211	0.196	0.180
	U^*=	0.809	0.799	0.789	0.778	0.768
11	h^*=	0.351	0.336	0.322	0.307	0.293
	U^*=	0.920	0.909	0.900	0.890	0.880
12	h^*=	0.468	0.453	0.438	0.423	0.408
	U^*=	1.208	1.018	1.008	0.998	0.989
13	h^*=	0.595	0.579	0.563	0.547	0.532
	U^*=	1.137	1.126	1.116	1.106	1.096
14	h^*=	0.734	0.715	0.698	0.681	0.664
	U^*=	1.247	1.235	1.224	1.214	1.203
15	h^*=	0.884	0.864	0.844	0.826	0.807
	U^*=	1.357	1.345	1.333	1.322	1.311
16	h^*=	1.047	1.024	1.003	0.982	0.962
	U^*=	1.469	1.456	1.443	1.431	1.420
17	h^*=	1.224	1.199	1.175	1.152	1.130
	U^*=	1.581	1.567	1.554	1.542	1.530
18	h^*=	1.414	1.386	1.360	1.334	1.310
	U^*=	1.695	1.680	1.666	1.653	1.640
19	h^*=	1.620	1.589	1.559	1.531	1.504
	U^*=	1.810	1.794	1.780	1.765	1.752
20	h^*=	1.840	1.806	1.773	1.742	1.712
	U^*=	1.926	1.909	1.894	1.878	1.864
21	h^*=	2.076	2.038	2.001	1.967	1.934
	U^*=	2.042	2.025	2.009	1.993	1.978

Tabular Solution Pertaining to the r^*-t^* Characteristic Network

NEGATIVE CHARACTERISTIC

PLUS CHARACTERISTIC

		29	30	31	32	33	34
10	h^*=	0.164	0.148	0.132	0.114	0.082	0.039
	U^*=	0.758	0.748	0.737	0.726	0.708	0.692
11	h^*=	0.279	0.862	0.250	0.236	0.212	0.189
	U^*=	0.871	0.862	0.852	0.843	0.829	0.812
12	h^*=	0.394	0.380	0.366	0.353	0.331	0.310
	U^*=	0.979	0.970	0.962	0.953	0.939	0.923
13	h^*=	0.517	0.502	0.488	0.474	0.452	0.431
	U^*=	1.087	1.077	1.068	1.060	1.046	1.030
14	h^*=	0.648	0.633	0.618	0.603	0.580	0.558
	U^*=	1.194	1.184	1.174	1.166	1.152	1.136
15	h^*=	0.790	0.773	0.757	0.741	0.716	0.693
	U^*=	1.300	1.291	1.281	1.272	1.257	1.241
16	h^*=	0.943	0.925	0.907	0.890	0.863	0.838
	U^*=	1.409	1.398	1.388	1.378	1.363	1.346
17	h^*=	1.109	1.088	1.069	1.050	1.021	0.994
	U^*=	1.518	1.506	1.496	1.485	1.469	1.451
18	h^*=	1.287	1.264	1.243	1.222	1.190	1.160
	U^*=	1.628	1.616	1.604	1.593	1.576	1.558
19	h^*=	1.478	1.453	1.430	1.406	1.371	1.339
	U^*=	1.738	1.726	1.714	1.702	1.684	1.665
20	h^*=	1.683	1.656	1.629	1.604	1.566	1.530
	U^*=	1.850	1.837	1.824	1.812	1.793	1.773
21	h^*=	1.902	1.872	1.843	1.815	1.773	1.733
	U^*=	1.963	1.949	1.936	1.923	1.903	1.881
22	h^*=	2.136	2.103	2.071	2.040	1.994	1.950
	U^*=	2.077	2.062	2.048	2.034	2.013	1.991
23	h^*=	2.384	2.348	2.313	2.279	2.228	2.180
	U^*=	2.192	2.176	2.161	2.147	2.125	2.102

Tabular Solution Pertaining to the r*-t* Characteristic Network

PLUS CHARACTERISTIC			NEGATIVE CHARACTERISTIC					
			35	36	37	38	39	40
10	h*=	0.025						
	U*=	0.653						
11	h*=	0.173	0.155	0.135	0.112	0.085	0.046	
	U*=	0.780	0.787	0.773	0.757	0.740	0.725	
12	h*=	0.295	0.280	0.264	0.246	0.227	0.207	
	U*=	0.913	0.901	0.889	0.876	0.862	0.246	
13	h*=	0.417	0.402	0.387	0.370	0.353	0.334	
	U*=	1.020	1.009	0.998	0.985	0.972	0.958	
14	h*=	0.544	0.529	0.513	0.497	0.480	0.462	
	U*=	1.125	1.114	1.103	1.091	1.078	1.064	
15	h*=	0.678	0.662	0.646	0.629	0.612	0.593	
	U*=	1.230	1.219	1.207	1.195	1.182	1.168	
16	h*=	0.822	0.805	0.788	0.770	0.751	0.732	
	U*=	1.335	1.323	1.311	1.298	1.285	1.271	
17	h*=	0.976	0.958	0.939	0.920	0.900	0.880	
	U*=	1.440	1.428	1.415	1.402	1.388	1.374	
18	h*=	1.141	1.121	1.101	1.080	1.059	1.037	
	U*=	1.546	1.533	1.520	1.506	1.492	1.477	
19	h*=	1.318	1.296	1.274	1.251	1.228	1.204	
	U*=	1.652	1.639	1.625	1.611	1.596	1.580	
20	h*=	1.506	1.483	1.458	1.434	1.408	1.382	
	U*=	1.759	1.746	1.731	1.716	1.701	1.685	
21	h*=	1.708	1.682	1.655	1.628	1.600	1.572	
	U*=	1.868	1.853	1.838	1.823	1.806	1.790	
22	h*=	1.922	1.893	1.864	1.834	1.804	1.773	
	U*=	1.977	1.962	1.946	1.930	1.913	1.895	
23	h*=	2.150	2.118	2.086	2.054	2.020	1.987	
	U*=	2.086	2.071	2.054	2.038	2.020	2.002	

Tabular Solution Pertaining to the r*-t* Characteristic Network

PLUS CHARACTERISTIC		NEGATIVE CHARACTERISTIC					
		41	42	43	44	45	46
11	h*=	0.006	0.003				
	U*=	0.704	0.528				
12	h*=	0.184	0.158	0.127	0.090	0.017	0.385
	U*=	0.829	0.809	0.787	0.760	0.753	0.864
13	h*=	0.315	0.293	0.270	0.245	0.216	0.184
	U*=	0.942	0.925	0.906	0.884	0.860	0.830
14	h*=	0.442	0.422	0.401	0.378	0.354	0.327
	U*=	1.049	1.032	1.014	0.994	0.972	0.946
15	h*=	0.574	0.554	0.533	0.511	0.487	0.463
	U*=	1.153	1.136	1.119	1.099	1.077	1.053
16	h*=	0.712	0.692	0.670	0.648	0.624	0.600
	U*=	1.255	1.239	1.221	1.202	1.180	1.156
17	h*=	0.858	0.837	0.814	0.791	0.767	0.742
	U*=	1.358	1.341	1.323	1.303	1.282	1.257
18	h*=	1.014	0.991	0.967	0.942	0.917	0.891
	U*=	1.461	1.443	1.425	1.405	1.382	1.357
19	h*=	1.180	1.154	1.129	1.102	1.076	1.048
	U*=	1.564	1.546	1.527	1.506	1.483	1.458
20	h*=	1.356	1.328	1.200	1.272	1.243	1.214
	U*=	1.667	1.649	1.629	1.608	1.584	1.558
21	h*=	1.543	1.513	1.483	1.452	1.421	
	U*=	1.772	1.752	1.732	1.710	1.686	
22	h*=	1.741	1.709	1.676	1.643		
	U*=	1.876	1.857	1.835	1.813		
23	h*=	1.952	1.917	1.881			
	U*=	1.982	1.962	1.940			
24	h*=	2.175	2.136				
	U*=	2.088	2.067				

Tabular Solution Pertaining to the r*-t* Characteristic Network

PLUS CHARACTERISTIC		NEGATIVE CHARACTERISTIC					
		47	48	49	50	51	52
12	h*=	0.064	0.000				
	U*=	1.323	1.470				
13	h*=	0.147	0.099	0.002			
	U*=	0.794	0.749	0.717			
14	h*=	0.298	0.267	0.232	0.193	0.146	0.096
	U*=	0.915	0.878	0.830	0.766	0.666	0.438
15	h*=	0.437	0.410	0.381	0.351	0.322	
	U*=	1.024	0.989	0.946	0.888	0.803	
16	h*=	0.575	0.549	0.523	0.497		
	U*=	1.127	1.094	1.052	0.997		
17	h*=	0.717	0.691	0.666			
	U*=	1.229	1.195	1.154			
18	h*=	0.865	0.839				
	U*=	1.329	1.295				
19	h*=	1.021					
	U*=	1.429					

Tabular Solution Pertaining to the r*-t* Characteristic Network

NEGATIVE CHARACTERISTIC

PLUS CHARACTERISTIC			21	22	23	24	25
21		h*=	2.205	2.159	2.116		
		U*=	2.100	2.080	2.061		
22		h*=		2.240	2.372	2.328	2.285
		U*=		2.200	2.180	2.161	2.142
23		h*=			2.645	2.596	2.549
		U*=			2.300	2.280	2.260
24		h*=				2.880	2.829
		U*=				2.400	2.380
25		h*=					3.125
		U*=					2.500

Tabular Solution Pertaining to the r*-t* Characteristic Network

NEGATIVE CHARACTERISTIC

PLUS CHARACTERISTIC

		26	27	28	29	30
22	h*=	2.245	2.207	2.171		
	U*=	2.125	2.108	2.092		
23	h*=	2.505	2.463	2.422	2.384	2.348
	U*=	2.242	2.225	2.208	2.192	2.176
24	h*=	2.780	2.734	2.690	2.648	2.608
	U*=	2.360	2.342	2.324	2.307	2.291
25	h*=	2.072	3.021	2.973	2.927	2.883
	U*=	2.480	2.460	2.442	2.424	2.407
26	h*=	3.380	3.325	3.272	3.222	3.174
	U*=	2.600	2.580	2.560	2.542	2.524
27	h*=		3.645	3.588	3.533	3.481
	U*=		2.700	2.680	2.660	2.642
28	h*=			3.920	3.861	3.804
	U*=			2.800	2.780	2.760
29	h*=				4.205	4.144
	U*=				2.900	2.880
30	h*=					4.500
	U*=					3.000

Tabular Solution Pertaining to the r*-t* Characteristic Network

NEGATIVE CHARACTERISTIC

PLUS CHARACTERISTIC			31	32	33	34	35
24	h*=	2.570	2.533	2.477	2.424	2.391
	U*=	2.276	2.260	2.237	2.213	2.197
25	h*=	2.842	2.801	2.740	2.683	2.646
	U*=	2.391	2.375	2.351	2.325	2.309
26	h*=	3.129	3.085	3.019	2.956	2.916
	U*=	2.507	2.490	2.465	2.438	2.421
27	h*=	3.432	3.384	3.312	3.244	3.120
	U*=	2.624	2.606	2.580	2.552	2.534
28	h*=	3.750	3.699	3.620	3.546	3.499
	U*=	2.742	2.724	2.696	2.667	2.649
29	h*=	4.085	4.029	3.945	3.864	3.813
	U*=	2.860	2.841	2.813	2.783	2.764
30	h*=	4.437	4.376	4.285	4.198	4.142
	U*=	2.980	2.960	2.930	2.900	2.879
31	h*=	4.805	4.740	4.641	4.547	4.487
	U*=	3.100	3.080	3.049	3.016	2.996
32	h*=		5.120	5.014	4.912	
	U*=		3.200	3.168	3.134	
33	h*=			5.645		
	U*=			3.360		

Tabular Solution Pertaining to the r*-t* Characteristic Network

PLUS CHARACTERISTIC			NEGATIVE CHARACTERISTIC				
			36	37	38	39	40
24	h*=		2.357	2.322	2.286	2.250	2.213
	U*=		2.181	2.164	2.146	2.128	2.109
25	h*=		2.609	2.571	2.532	2.492	2.452
	U*=		2.292	2.274	2.256	2.237	2.217
26	h*=		2.875	2.833	2.791	2.748	2.704
	U*=		2.404	2.385	2.366	2.346	2.325
27	h*=		3.155	3.110	3.064	3.017	
	U*=		2.516	2.497	2.477	2.456	
28	h*=		3.450	3.401	3.351		
	U*=		2.629	2.610	2.589		
29	h*=		3.760	3.707			
	U*=		2.744	2.723			
30	h*=		4.085				
	U*=		2.858				

Tabular Solution Pertaining to the r*-t* Characteristic Network

			NEGATIVE CHARACTERISTIC	
			41	42
PLUS CHARACTERISTIC	24	h*=	2.175	2.136
		U*=	2.088	2.067
	25	h*=	2.410	
		U*=	2.196	